Antimicrobial Peptide-Lipid Binding Interactions and Binding Selectivity

Mitaben D. Lad,* Fabrice Birembaut,* Luke A. Clifton,* Richard A. Frazier,* John R. P. Webster,† and Rebecca J. Green*

*School of Chemistry, Food Biosciences and Pharmacy, University of Reading, Whiteknights, Reading RG6 6AD, United Kingdom; and †Council for the Central Laboratory of the Research Councils, Rutherford Appleton Laboratory, Didcot, United Kingdom

ABSTRACT Surface pressure measurements, external reflection-Fourier transform infrared spectroscopy, and neutron reflectivity have been used to investigate the lipid-binding behavior of three antimicrobial peptides: melittin, magainin II, and cecropin P1. As expected, all three cationic peptides were shown to interact more strongly with the anionic lipid, 1,2 dihexadecanoyl-*sn*-glycerol-3-(phosphor-rac-(1-glycerol)) (DPPG), compared to the zwitterionic lipid, 1,2 dihexadecanoyl-*sn*-glycerol-3-phosphocholine (DPPC). All three peptides have been shown to penetrate DPPC lipid layers by surface pressure, and this was confirmed for the melittin-DPPC interaction by neutron reflectivity measurements. Adsorption of peptide was, however, minimal, with a maximum of 0.4 mg m^{-2} seen for melittin adsorption compared to 2.1 mg m^{-2} for adsorption to DPPG (from 0.7 μM solution). The mode of binding to DPPG was shown to depend on the distribution of basic residues within the peptide α-helix, although in all cases adsorption below the lipid layer was shown to dominate over insertion within the layer. Melittin adsorption to DPPG altered the lipid layer structure observed through changes in the external reflection-Fourier transform infrared lipid spectra and neutron reflectivity. This lipid disruption was not observed for magainin or cecropin. In addition, melittin binding to both lipids was shown to be 50% greater than for either magainin or cecropin. Adsorption to the bare air-water interface was also investigated and surface activity followed the trend melittin>magainin>cecropin. External reflection-Fourier transform infrared amide spectra revealed that melittin adopted a helical structure only in the presence of lipid, whereas magainin and cecropin adopted helical structure also at an air-water interface. This behavior has been related to the different charge distributions on the peptide amino acid sequences.

INTRODUCTION

Antimicrobial peptides have been designed by nature to be highly selective in their mode of interaction with imposing microbes. Their unique property has been identified as their ability to target the outer membrane in bacterial cells, thereby disrupting the electrochemical gradient across the cell, leading to the loss of cell integrity and function (1–3). With the current increase in resistance to conventional antibiotics, the high degree of selectivity possessed by antimicrobial peptides makes them suitable candidates for the development of future antibiotics. Membrane selectivity varies for different peptides (4–6), where they either selectively interact with eukaryotic or prokaryotic cell membranes (3,7,8). They are classified as prokaryotic active peptides, e.g., magainin, cecropin, and defensin; eukaryotic active peptides, e.g., δ-hemolysin, gramicidin A, and cinnamycin; and nonmembrane-selective peptides, e.g., melittin (MLT) and pardaxin. Several mechanisms of adsorption have been reported to occur: the Barrel-Stave, the torroid pore or wormhole, and the carpet mechanisms (8–10). The one common feature of all these mechanisms is the initial predominant electrostatic interaction that drives the peptide to bind to the lipid layer. The sequence of events that follows subsequently varies for different peptides and lipid. Among others, magainin and MLT have been shown to adopt an α-helical conformation in the presence of lipids, which is in contrast to the extended conformation that the peptides adopt in solution (11,12).

MLT is one of the most widely studied peptides (11,13–17). It is isolated from honeybee (*Apis mellifera*) venom and has 26 amino acid residues and a net positive charge at physiological pH (18). The lack of membrane selectivity of MLT has been related to the amino acid sequence and in turn the tertiary structure of the peptide (19). MLT's interaction with lipids has been investigated using a range of methodologies, including NMR (9,14), circular dichroism (10,15), surface plasmon resonance (11,16), and attenuated total reflectance-infrared (IR) spectroscopy (13,17). Because of its nonselectivity, MLT is an interesting choice for study to understand the mechanisms of adsorption, although past studies have not reached a clear consensus on the conformation of the peptide in or adsorbed to lipid bilayers. The use of the above spectroscopic techniques has shown that the peptide interacts more strongly in the presence of anionic lipids than those that are zwitterionic in charge, where the driving force of interaction is believed to be electrostatic. MLT has also been shown to adopt an α-helical conformation in the presence of lipids, which is in contrast to the extended conformation that the peptide adopts in solution (10). This conformational change of MLT is important in its mechanism of interaction, i.e., pore formation. Studies to date have been key to the understanding of the structural effects of both the lipid layer and peptide on interaction. However, the initial interaction of the peptide with a lipid membrane and subsequent effect on the structure of the lipids has seldom been discussed.

Submitted September 21, 2006, and accepted for publication January 22, 2007.

Address reprint requests to Rebecca J. Green, Fax: 44-118-378-6331; E-mail: rebecca.green@rdg.ac.uk.

0006-3495/07/05/3575/12 $2.00

doi: 10.1529/biophysj.106.097774

Of the membrane-selective peptides, magainin has been widely studied and reported to form pores at cell membranes (12,20,21). The orientation of magainin penetration into the lipid layer has been studied by a variety of techniques to investigate the mechanism of interaction that leads to cell death. This has led to the consensus that the peptide interacts and kills the cells by penetrating the membrane structure by arranging perpendicular to the lipid interface and adopting a helical conformation (20–22). Research has shown that the interaction is stronger if the lipid layer is anionic and that a critical concentration of peptide in the surface region appears to be required before pore formation and cell death occur (20,22–24). However, other mechanisms leading to cell death may also exist where pore formation is not necessary, one such being the carpet mechanism, which has been proposed as the method of cell attack for the peptide cecropin P1 (CEC) (25–29). The proposed binding mechanism has been linked to the peptide's helical structure on contact with the lipid vesicle. Unlike cecropins A, B, and D, CEC does not have a helix-bend-helix structure that occurs due to a central proline residue. Instead, CEC forms a continuous helix, with a proline existing near its C-terminus. The single helix structure provides less flexibility, and this is believed to inhibit penetration into the lipid structure (28,29). It is therefore believed to disrupt the membrane structure by interacting with the lipid headgroup parallel to the membrane surface, creating a leaky membrane structure and ultimately cell death.

To gain insight into peptide-membrane interaction, the biological membrane has been experimentally modeled using lipid vesicles, monolayers, and surface-bound multilayers (17,20,30,31). Measurements using lipid monolayers have been shown to be effective for investigating protein-lipid interactions because the lipid layer composition and compression can be carefully controlled (32). Research has shown that surface pressure measurements and external reflection-Fourier transform infrared (ER-FTIR) spectroscopy (also known as IRRAS, infrared reflection absorption spectroscopy) are effective tools in studying the interaction between proteins and lipids (33–35). Both methods are sensitive to adsorption processes at the air-liquid interface, and thus synergy in experimental design enables the techniques to be used in a complementary manner. Surface pressure measurements are highly sensitive to peptide penetration of lipid layers, but less so to adsorption below the lipid layer. ER-FTIR spectroscopy can be used to observe the structural impact on the lipid molecules as the peptide adsorbs and changes in peptide secondary structure. The lipid layer structure is observed by monitoring the CH peaks of the lipid acyl chains, and the adsorption of and structural change in the peptide is observed by the presence of an amide I peak (34,36). The authors' previous work has used these methods to investigate protein-lipid interactions and in the study of protein conformational change during adsorption to the air-water interface (36,37).

A further suitable complementary tool to ER-FTIR spectroscopy is neutron reflectivity (NR) (38). Studies of lipid monolayers using this method have been carried out showing the technique to be sensitive to structure and orientation of the lipid molecules (39). NR provides a means of quantitatively determining adsorbed layer structure at the air-water interface and differentiating between interfacial species. Thus it provides a method of probing the position and concentration of peptide within the lipid layer.

It is possible that a single peptide can interact with a membrane surface in more than one way, possibly enabling a single type of peptide to attack a membrane via more than one mode of interaction. Such processes may well be linked to the lack of membrane selectivity seen for some antimicrobial peptides. We have taken three complementary methods, surface pressure measurements, ER-FTIR spectroscopy, and NR, to provide information on the initial peptide-lipid interaction. These methods are used to determine changes in peptide and lipid layer structure as a result of different peptide-lipid interaction and to differentiate between different modes of interaction. Three peptides have been investigated, MLT, magainin II, and CEC, where contrasting lipid-binding behavior is expected. Differences in binding behavior of these peptides to the bare air-water interface and zwitterionic and anionic lipids have been observed and related to peptide structure.

MATERIALS AND METHODS

Materials

Lipids were obtained from Avanti Polar Lipids (Alabaster, AL) and peptides from American Peptide (Sunnyvale, CA), and all were used as supplied. The solutions of 1,2 dihexadecanoyl-*sn*-glycerol-3-phosphocholine (DPPC) (synthetic purity >99%) with a molecular mass (MM) of 734 g mol^{-1} and 1,2 dihexadecanoyl-*sn*-glycerol-3-(phosphor-rac-(1-glycerol)) (DPPG) (sodium salt) (synthetic purity >99%) with an MM of 745 g mol^{-1} were prepared in chloroform (Sigma, St. Louis, MO; 99%+) to a concentration of 0.5 g dm^{-3}. MLT (MM = 2847 g mol^{-1}) is a 26-residue hemolytic peptide isolated from the venom of European honeybee *A. mellifera* (18). Magainin II (MGN) (MM = 2466 g mol^{-1}) is a 23-residue antimicrobial peptide isolated from African frog skin (5). CEC (MM = 3339 g mol^{-1}) is a 31-residue antimicrobial peptide isolated from porcine intestine (40). The peptide solutions were made using a phosphate buffer solution of pH 7 (I = 0.02 M) using UHQ grade water. Peptide solutions were diluted to the required concentration (0.088–3.5 μM) through adding concentrated peptide solutions to the 80-cm^3 buffer subphase of the Langmuir trough. For the FTIR experiments the peptide solution was made in a D_2O phosphate buffer 24 h in advance to allow for deuterium-hydrogen exchange to equilibrate.

Surface pressure measurements

Lipid monolayers were created at the air-water interface using a Langmuir trough (model 611, Nima Technology, Coventry, England). Surface pressure measurements were carried out by the Wilhelmy plate method; this consisted of a strip of chromatography work in contact with the aqueous subphase and linked to a balance (surface pressure sensor). Before the start of an experiment the trough and the barriers were thoroughly cleaned with UHQ grade water and chloroform. The trough was filled with 80 cm^3 buffer solution (pH 7, I = 0.02 M) onto which 20 μl of a 0.5 g dm^{-3} solution of lipid was spread. After allowing time for the chloroform to evaporate, the lipid layer was compressed and held at the required surface pressure. The compressed lipid layers were measured as surface pressure (π)-area (A)

curves and held at the desired surface pressure by fixing the barriers. Peptide solution (2 cm^3) was introduced into the subphase via a custom-made metal tube fixed below the buffer surface. Peptide solution was added into the tube using a syringe and dispersed within the subphase through a series of small holes along the length of the tube (36,37). This method of peptide addition allowed for rapid mixing and even distribution of peptide solution in the subphase without disturbing the lipid monolayer. On addition of peptide solution to the subphase, plots of surface pressure versus time were recorded to follow adsorption of peptide to the lipid layer. All data were repeated and found to be consistent with final surface pressure values with a standard deviation of ± 1 mN m^{-1}.

FTIR spectroscopy

FTIR spectra were recorded using a Thermo Nicolet Nexus (Madison, WI) fitted with a liquid nitrogen cooled mercury cadmium telluride detector and an air dryer to purge the instrument of water vapor and carbon dioxide. Lipid-peptide interactions were measured by ER using a monolayer/grazing angle accessory (Specac 19650 series, Kent, England). The accessory was also equipped with a small PTFE trough (94 × 22 × 5 mm), which was filled with deuterated buffer and fitted onto the grazing angle accessory before starting the experiment. The ER accessory was aligned such that the angle of incidence was 45°. Access to the Teflon trough throughout the experiment was via a small sliding lid to maintain the dry air purge. All FTIR spectra were recorded at a resolution of 4 cm^{-1} where 265 interferograms were collected and coadded and were ratioed against a background spectrum of D_2O buffer solution. All data were successfully reproduced. The FTIR procedure was followed as described previously (36).

Neutron reflectivity

NR measurements were carried out using the white beam SURF reflectometer at the Rutherford Appleton Laboratory (Oxfordshire, UK), using neutron wavelengths from 0.5 to 6.5 Å. The Langmuir trough arrangement described above for the surface pressure measurements was used and mounted onto an antivibration table within the sample environment of the reflectometer. The collimated neutron beam was reflected at the air-liquid interface at two different glancing angles of incidence: 1.5° and 0.8°. The beam intensity was calibrated with respect to clean D_2O. A flat background was determined by extrapolation to high values of momentum transfer, κ ($\kappa = (4\pi \sin\theta)/\lambda$, where λ is wavelength and θ is the incident angle).

Specular NR is largely determined by the variation in scattering length density along the surface normal (41). Different isotopes have different scattering lengths, and thus isotopic substitution can be used to produce a variety of NR profiles corresponding to a single number density profile providing a means of determining the composition of multi-component systems such as the peptide-lipid system reported here. A detailed description of the procedure used to obtain and fit NR profiles is given for protein-surfactant systems in previous publications (42–44) and thus is described only briefly here. Lipid layers were prepared as described above using surface pressure changes to monitor compression, and NR profiles were obtained for equilibrated systems before and after addition of peptide to the aqueous subphase. Null reflective water (NRW) (8% D_2O) was used as the aqueous subphase such that the reflectivity profile was sensitive to the interfacial region only (42). Reflectivity curves were repeated using both chain hydrogenated and chain deuterated lipids to provide isotopic contrast between the lipids and peptides at the surface.

The resulting reflectivity profiles have been analyzed using the optical matrix formalism, which has been described in detail elsewhere (45). A typical modeling procedure calculates the reflectivity based on fitting to the structural parameters: number of layers, thickness, and corresponding scattering length density of each layer. A set of reflectivity profiles measured under different isotopic compositions, n, are fitted to the same layer and thickness model with the scattering length density varying, depending on the density and composition of the lipid-peptide interface. The fitted scattering length density for each isotopic contrast, ρ_n, can be related to the volume fraction of each component in the system by $\rho_n = \rho_{peptide}\,\phi_p + \rho_{lipid\ (H\ or\ D)}\,\phi_{lipid} + \rho_{water}\,\phi_{water}$. In these experiments NRW is used and, thus, $\rho_{water}\,\phi_{water} = 0$. An equation for each isotopic contrast, using hydrogenated or deuterated lipid, provides enough information to solve the resulting equation for volume fractions, ϕ. Therefore, area per molecule and surface excess can be determined for each interfacial species. For example, if the lipid layer is contrast matched to the NRW subphase (i.e., nonreflecting), the resulting reflectivity profile will come from the peptide contribution only and thus the modeled scattering length density will be proportional to the volume fraction of the peptide. Thus, the volume density and the surface excess of the lipid and protein within each layer can be distinguished (42).

RESULTS

Peptide binding to the bare air-water interface

Initially, surface pressure measurements and ER-FTIR spectra were recorded for antimicrobial peptide adsorption (0.7 μM) to the bare air-water interface, as shown in Fig. 1 *a*. Adsorption to the bare air-water interface gave a similar surface pressure profile for all three peptides. After addition of peptide to the substrate, an induction period of up to 40 min was present before any increase in surface pressure was observed. This induction period was followed by a sharp increase and then plateau before a final surface pressure increase of 23, 21, and 18 mN m^{-1} was observed for MLT, MGN, and CEC, respectively. Induction periods have been observed in surface pressure data previously and have been explained in terms of orientation changes in the adsorbed protein layer, rather than due to delayed adsorption. It should be noted that surface pressure data describe the ability of the adsorbed material to change the surface tension of the interface, rather than adsorbed amount (36,46).

Indeed, some studies have shown that, for protein adsorption, a 50% adsorbed molecular layer is required before an increase in surface pressure is observed (46). Our ER-FTIR data confirmed these observations, showing an increase in the peptide amide I peak within seconds of peptide addition to the subphase as shown by the amide I peak area data in Fig. 1 *b*. Final spectra are given in Fig. 1 *c* showing differences in the peak shape, and therefore the secondary structure, for each peptide. Two observations can be made: First, although the adsorption rate is different for the two methods, the trend in terms of final adsorbed peptide layer is the same with CEC<MGN<MLT. Second, deconvolution of the amide I peak suggests that MGN has a high helix confirmation (peak max at 1650 cm^{-1}) at the interface, compared to MLT where no evidence of helix is seen, with a peak maximum at 1640 cm^{-1} indicative of random coil structure. As will be discussed later the peak maximum observed for MLT is in apparent contrast to the 1656 cm^{-1} peak maximum observed by Cornut et al. (32).

Peptide binding to DPPC and DPPG lipid monolayers

Fig. 2 shows surface pressure against time plots for peptide adsorption (0.7 μM) to the air-buffer interface in the

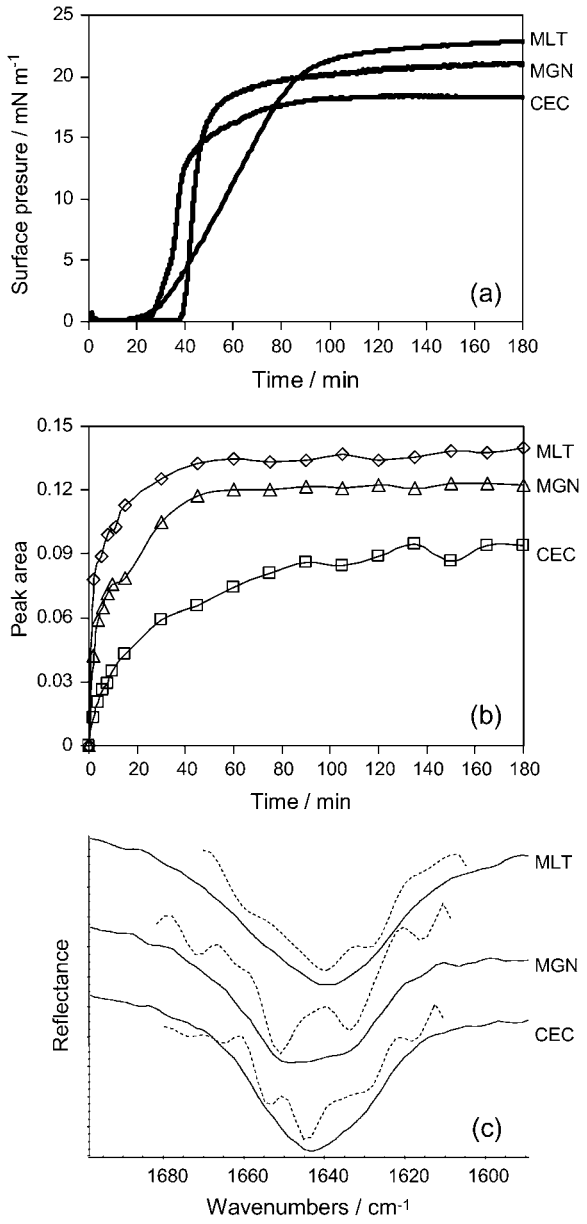

FIGURE 1 Surface pressure and ER-FTIR data for antimicrobial peptide adsorption to the air-water interface. Plot *a* shows surface pressure versus time after addition of each peptide to the aqueous subphase at time = 0. Plot *b* shows peptide adsorption as followed by ER-FTIR spectroscopy, giving the increase in amide I peak area versus time. Plot *c* shows the amide I spectra for each peptide after adsorption for 3 h where the dotted lines give the deconvoluted amide I peaks.

presence of a lipid layer over a 3-h period. The results for the three antimicrobial peptides, MLT, MGN, and CEC, are shown. In the presence of a condensed DPPC or DPPG layer (20 mN m^{-1}), no delay in surface pressure increase was observed. To DPPC, surface pressure change was rapid, leading to a final increase in surface pressure of 10, 5, and 3 mN m^{-1} for MLT, MGN, and CEC, respectively. In the presence of a DPPG monolayer, the increase in surface pressure was greater, due to the stronger electrostatic interaction between the cationic peptide and anionic lipid headgroup. Final surface pressure increases were 20, 12, and 9 mN m^{-1} for MLT, MGN, and CEC, respectively. The nonselective peptide, MLT, gave a greater increase in surface pressure and thus greater reduction in surface-free energy to both lipid surfaces compared to the membrane-selective peptides.

Fig. 3 shows the CH stretch and amide I regions of the ER-FTIR spectra for MLT, MGN, and CEC (0.7 μM) interaction with a condensed DPPC monolayer recorded over a 3-h period. Three peaks were observed in the CH stretch region: a CH_3 stretch (2958 cm^{-1}) and asymmetric and symmetric CH_2 stretches (2918 cm^{-1} and 2850 cm^{-1}, respectively). In the amide region, a CO stretch was observed at 1740 cm^{-1} due to the headgroup carbonyl of the lipid, but the amide I peak (1650 cm^{-1}) expected upon peptide adsorption was not observed. The amide I peak was absent over the full 3-h duration of the experiment and suggests that no peptide adsorbed to the interface, which appears to contradict the surface pressure data. In addition, no change in the lipid CH and CO stretch peak sizes or positions is observed, suggesting that the lipid structure does not significantly alter when the peptide is introduced to the system. In systems where protein binding is observed, changes in the intensity of the CH stretch vibrations have been observed and related to changes in average lipid chain tilt angle (47).

ER-FTIR spectra, corresponding to the CH stretch and amide spectral regions, for MLT, MGN, and CEC binding to a condensed DPPG monolayer are shown in Fig. 4. For MLT, adsorption was observed for a 3-h period using a solution concentration of 0.7 μM. For MGN and CEC, the first 2 h of adsorption was at a concentration of 0.7 μM; the peptide concentration was then increased to 3.5 μM for a further 3 h. The spectra shown in Fig. 4 are representative of a large data set, where spectra were recorded regularly throughout the adsorption period and experiments repeated three or more times.

Fig. 4 *a* shows spectra for MLT adsorption to DPPG. In these spectra, CH stretch and CO stretch peaks corresponding to the lipid layer and an amide I peak corresponding to peptide adsorption were observed. During peptide adsorption, changes in peak area and position were observed in the CH and CO stretch vibrations of the lipid. The CH_3 stretch vibration broadened and shifted position from 2958 to 2962 cm^{-1}, but its peak area did not change. Both the CH_2 asymmetric and the CO stretch vibrations broadened during peptide adsorption, resulting in reduced peak area (see peak areas shown in Fig. 5). These changes can be attributed to changes of the lipid layer structure and orientation caused by the MLT interaction that led to either increased tilt angle of the lipid layer (47) or decreased molecular order of the lipid structure. MLT adsorption was observed as a gradual increase in amide I peak area during the 3-h adsorption time, but the shape of the peak did not significantly alter throughout the adsorption period. Although the surface pressure

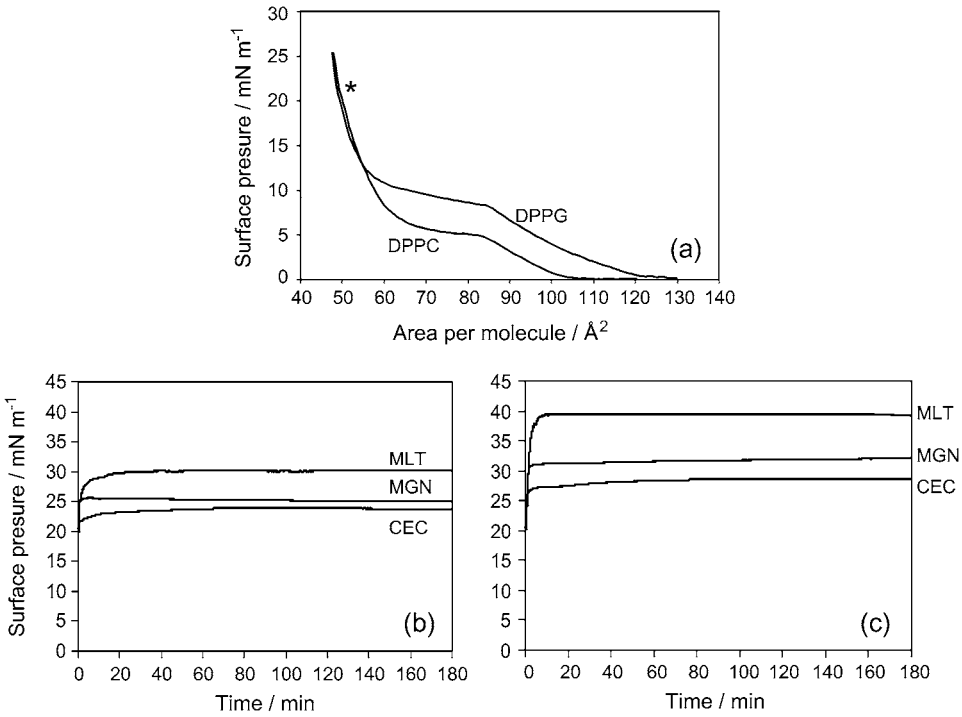

FIGURE 2 Surface pressure data for peptide binding to DPPC and DPPG lipid monolayers. Plot *a* gives the π-*A* curves. The asterisk indicates the condensed phase of the lipids at which compression all peptide adsorption experiments were carried out. Plots *b* and *c* show the surface pressure versus time data upon addition of peptide to (*b*) DPPC and (*c*) DPPG.

kinetics was quite rapid for MLT adsorption to DPPG (Fig. 2), adsorption was shown to be far slower by FTIR spectroscopy. Due to the insensitivity of surface pressure changes to interactions below the uppermost lipid layer, this observation suggests that adsorption of MLT below the DPPG layer occurs as well as penetration of the lipid layer.

For MGN and CEC (Fig. 4, *b* and *c*), adsorption occurred rapidly, as observed by the appearance of an amide I peak at ~1650 cm^{-1}. Unlike MLT, the CH and CO stretch vibrations resulting from the lipid monolayer were not affected by the addition of peptide. Increasing the concentration of peptide appeared to have little effect on the amide I peak height or shape. Fig. 6 provides peak area data for the CH_2 (2918 cm^{-1}) and the amide I (1650 cm^{-1}) peaks for MGN and CEC. This shows the change in peak area for the data shown in Fig. 4 and also for repeat experiments of peptide adsorption from a 0.7 μM solution for 3 h. The repeat data provide evidence of the repeatability of the data in terms of stability of the lipid layer and peptide adsorption.

The rates of increase of the amide I peak areas for MGN and CEC were shown to be rapid compared to MLT, with adsorption twice as fast for MGN (plateaus after 20 min) compared to CEC (plateaus after 40 min adsorption). In addition, the rate appears slower than the rate of change in surface pressure shown in Fig. 1. Surface pressure values resulted in a plateau after <5 min adsorption time. The FTIR data also showed that increasing the concentration fivefold resulted in no further adsorption of peptide. However, adsorption of CEC at 0.35 μM resulted in ~50% adsorption compared to a 0.7 μM solution (data not shown). Therefore, maximum interaction can be assumed at the concentrations presented in this work.

The amide I peak shape is indicative of peptide secondary structure and was seen to be markedly different for the three

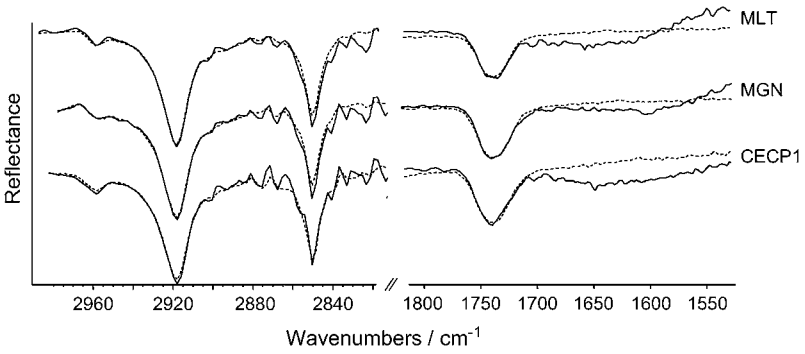

FIGURE 3 ER-FTIR spectra for peptide interactions with condensed phase DPPC monolayers. For each peptide, the dotted line shows the spectra just before peptide addition and the solid line after 3 h adsorption. Spectra were recorded at regular intervals throughout the 3-h adsorption period. (Spectra are offset but represented on same scale with full scale of reflectance axis of −0.16.)

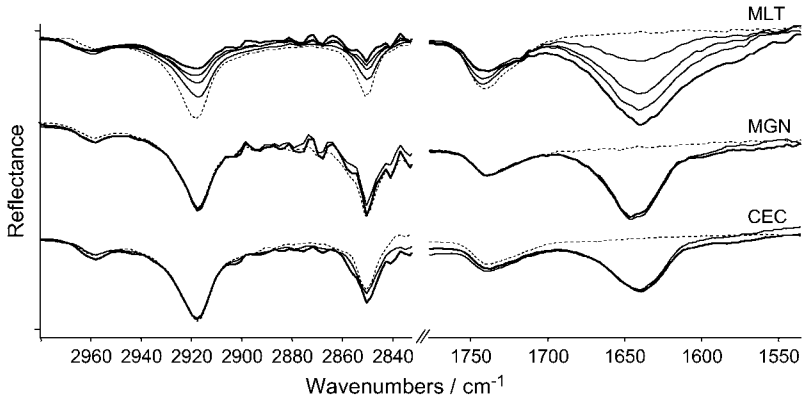

FIGURE 4 ER-FTIR spectra for peptide interactions with condensed phase DPPG monolayers. For each peptide, the dotted line shows the spectra just before peptide addition. MLT adsorption (from 0.7 μM solution) was recorded over a 3-h period and spectra are shown for 15 min and 1, 2, and 3 h (*bold line*) adsorption. For MGN and CEC, spectra are shown after 2 h adsorption from a 0.7 μM solution and after a further 3 h adsorption at an increased solution concentration of 3.5 μM. Spectra were recorded at regular intervals throughout the adsorption period. (Spectra are offset but represented on same scale with full scale of reflectance axis of −0.24.)

peptides (as seen in Figs. 5 and 6). For MLT adsorption to the air-water interface, a peak centered at 1640 cm^{-1} was observed, suggesting a random coil structure. In the presence of a DPPG lipid layer, a shoulder at 1652 cm^{-1} was also evident; this shoulder is a result of an increased α-helix structure in the presence of the DPPG monolayer (48). MGN exhibited a strong helix confirmation at both surfaces, as seen from the 1650 cm^{-1} maxima revealed by peak deconvolution (Fig. 6). In contrast, for CEC the dominant feature occurred at ~1640 cm^{-1}, suggesting a higher random coil component for the adsorbed peptide structure. Interestingly, no significant structural differences were observed for MGN and CEC when comparing adsorption at a DPPG layer to adsorption at the bare air-water interface. This helical structure associated with peptide interaction with lipids has been shown in previous studies, but has not been reported to occur when lipid is not present (21,28). For MLT, our observation showing a peak maximum at 1640 cm^{-1} is in apparent contrast to a previous study at the air-water interface using PMIRRAS by Cornut et al. (32), where a peak maximum of 1656 cm^{-1} was observed. The experimental conditions of these two studies are significantly different, with these data using a D_2O subphase, displaying a superior signal/noise ratio that has enabled peak deconvolution, and representing the adsorbed state after 3 h (rather than 20 min) adsorption.

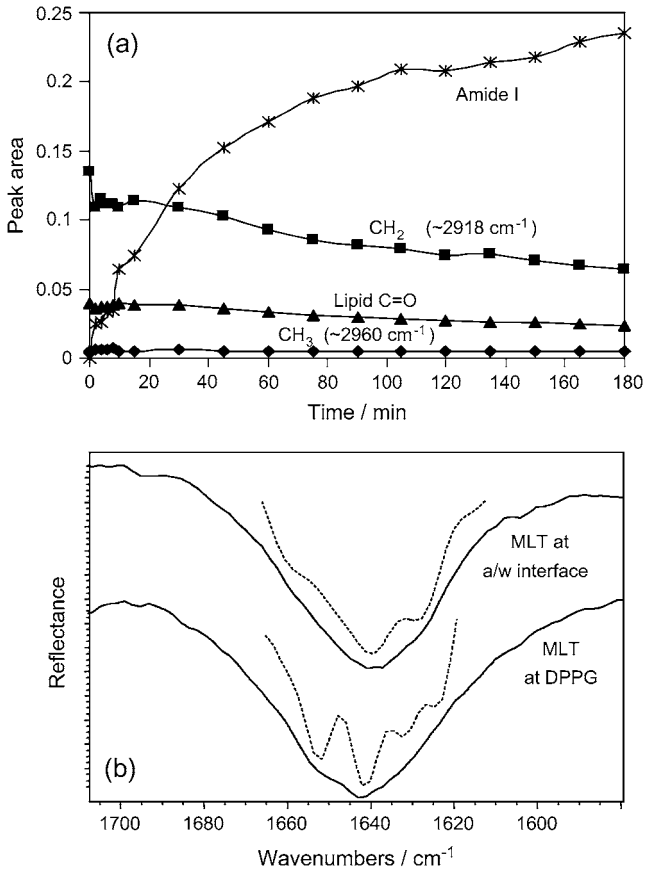

FIGURE 5 Peak area (plot *a*) and amide I peak deconvolution (plot *b*) data taken from the ER-FTIR spectra recorded for MLT adsorption to a condensed DPPG monolayer. The dotted lines in plot *b* show the peak deconvolution of the amide I peak for MLT adsorption to the air-water interface both with and without the presence of DPPG.

Figs. 7 and 8 provide NR curves for peptide binding to DPPG. Fits are also provided and are summarized in Tables 1 and 2. As described in the Materials and Methods section, deuteration provides a means of highlighting particular features within an interfacial layer. Table 1 provides fitting data to reflectivity curves for the equilibrium adsorption of all three peptides to a hydrogenated DPPG monolayer. Under these conditions the scattering length density of the DPPG is low (3.6×10^{-7} A^{-2}) and therefore we can approximately determine the surface excess of each peptide at the interface (42). These calculations have shown that, as seen with the previous methods, the extent of interaction is CEC<MGN <MLT. The data also suggest that the film thickness is greater for MLT (42 Å) compared to 30 Å for CEC and MGN. Table 1 also shows data for adsorption of MLT at lower concentrations.

The use of deuterated lipid enables the position of the peptide and the lipid at the interface to be determined (42). This is achieved by fitting data from experiments using both deuterated and hydrogenated lipid as described above. Fig. 7 shows the reflectivity profiles of a chain-deuterated DPPG

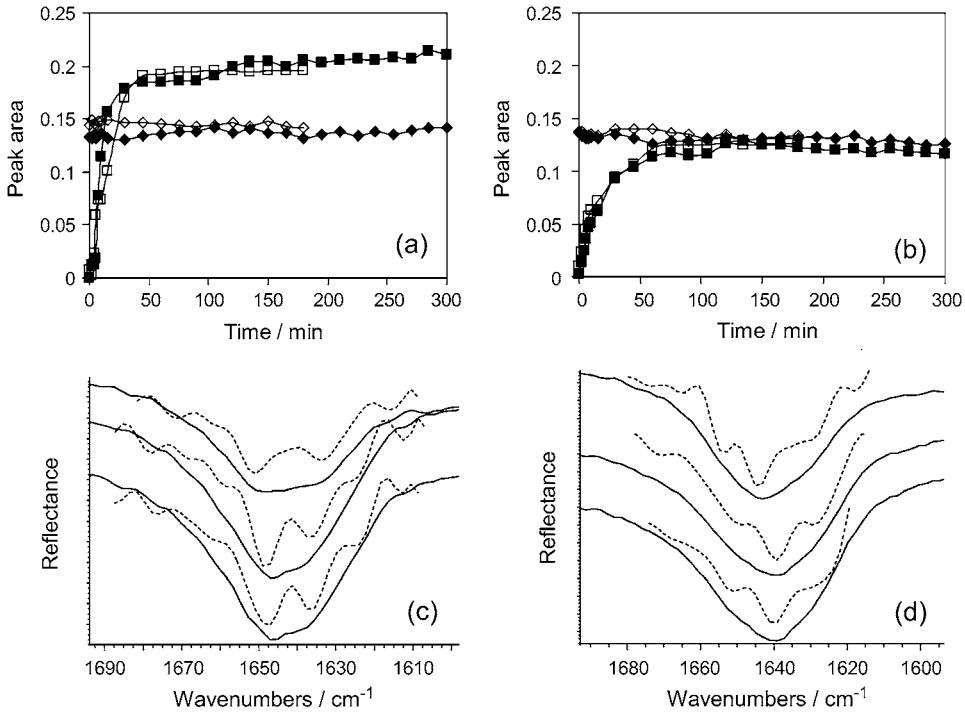

FIGURE 6 Amide I (*square symbol*, 1650 cm^{-1}) and CH_2 (*diamond symbol*, 2920 cm^{-1}) peak area verses time plots for MGN (*a*) and CEC (*b*) adsorption to condensed DPPG monolayers. Solid symbols represent the data taken from spectra shown in Fig. 4, and the open symbols indicate repeat data. Amide I peak deconvolution for the final spectra are shown in plots (*c*) MGN and (*d*) CEC for adsorption to the bare air-water interface (0.7 μM) (*top*) and to the DPPG monolayer at 0.7 μM (*middle*) and 3.5 μM (*bottom*) solution concentrations.

lipid layer and profiles for MLT and MGN adsorption to both a hydrogenated (h)- and chain deuterated (d)-DPPG layer in NRW. The deuterated (d)-DPPG-peptide (NRW) reflectivity profile is sensitive to both species at the interface. Adsorption from a 0.7 μM MLT solution is given in Fig. 7 *a*. This figure shows that the (d)-DPPG-MLT reflectivity profile is lower (less dense) than the pure (d)-DPPG profile, suggesting that the density of the lipid layer has been reduced and, thus, the ordering of lipid layer has been significantly altered. A fringe (curve inflection) also appears as a result of MLT adsorption, which indicates an increase in layer thickness. Therefore, before fitting these data, we can deduce that the peptide adsorbs in a manner that thickens the interfacial layer and disrupts the lipid layer structure.

Fitting the pure (d)-DPPG layer to a single layer model resulted in an area per molecule for the lipid of 55 $Å^2$, in agreement with surface pressure and literature values (49). Compression of (d)-DPPG follows a slightly different surface pressure-area curve than that for (h)-DPPG due to differences in interactions between deuterated hydrocarbon chains compared to hydrogenated chains (38). This is particularly apparent within the phase transition period between 65–80 $Å^2$/molecule. At 20 mN m^{-1}, both lipid layers are compressed within equivalent phase states. A simple single layer model was, however, not sufficient to fit the DPPG-MLT data, shown in Fig. 7 *a*, such that the reflectivity curves for the two isotopic contrasts fitted to the same physical model. A three-layer model was required, and the fitting parameters are shown (Table 2). Since the layer structure has proven to be complicated, these fits may not be unique, and further NR studies using additional isotopic contrasts would be required to confirm the model. However, the surface excess data are likely to be consistent and largely independent of the model used and, therefore, certain conclusions about the interaction between MLT and DPPG can be made. The model suggests a total adsorbed amount of peptide to be 2.1 mg m^{-2}, situated both within the upper lipid layer and immediately below the lipid. The model also suggests that the concentration of the lipid component reduces by 25% within the upper layer, existing as a more diffuse structure within the lower surface layers.

Fig. 7, *b* and *c*, shows the NR curves and the corresponding fits for MLT adsorption to DPPG at 0.175 and 0.088 μM solution concentrations of MLT. If the concentration of peptide was reduced from 0.7 to 0.175 μM, a two-layer model could be used to fit the data showing a surface concentration of MLT of 1.1 mg m^{-2} situated within the upper lipid layer (Table 2). The lipid layer is distorted at this MLT concentration with 17% of the lipid existing as a diffuse layer below the upper lipid monolayer. At an MLT concentration of 0.088 μM, the disruption in the lipid layer was no longer observed, and a single layer model could be used to fit the data successfully, resulting in a surface excess of MLT of 0.6 mg m^{-2}. The single layer fit suggests that the MLT resides within (penetrates) the lipid layer rather than adsorbing below the layer. Therefore, disruption of the lipid layer and significant adsorption of peptide below the lipid layer appear to be dependent on MLT concentration. At low concentrations, peptide penetrates the DPPG layer without affecting the structural order of the lipid. Even at one-eighth

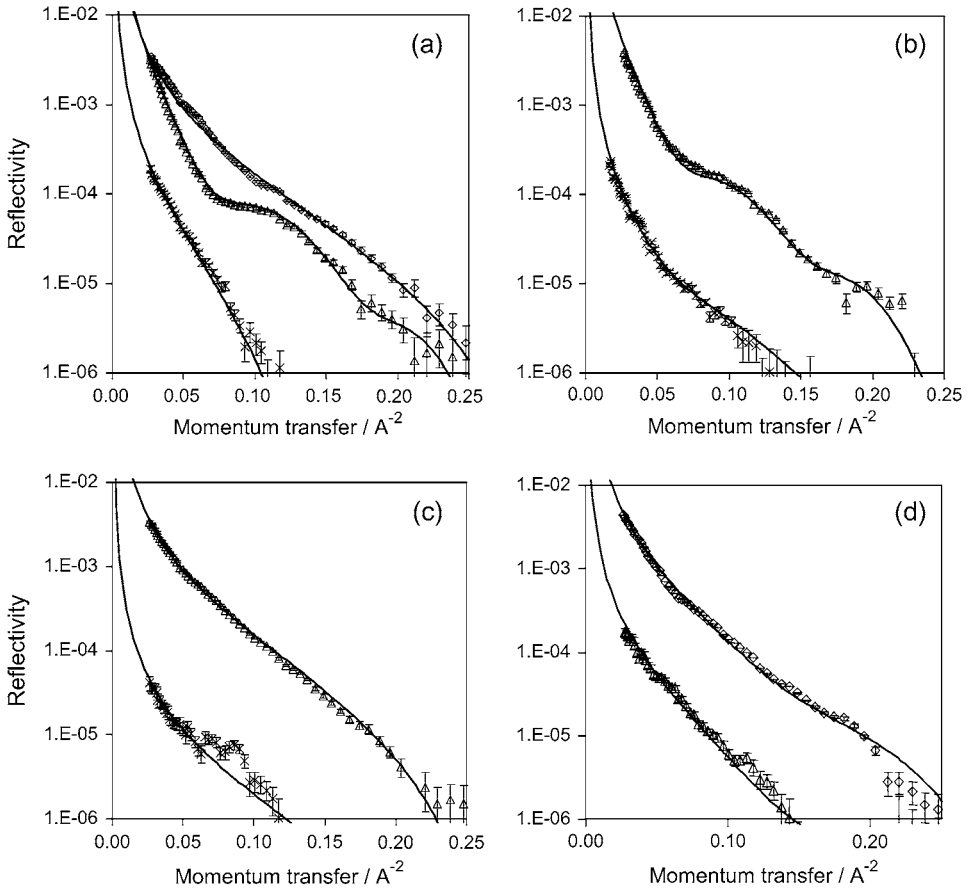

FIGURE 7 NR versus momentum transfer plots for 0.7 μM (plot *a*), 0.175 μM (plot *b*), 0.088 μM (plot *c*) MLT, and 0.7 μM (plot *d*) MGN adsorption to a condensed DPPG monolayer. For each plot, reflectivity profiles for peptide adsorption to chain deuterated (*triangles*) and hydrogenated (*crosses*) DPPG are shown. Diamond symbols represent the deuterated-DPPG monolayer before peptide addition, and solid lines give best model fits to the data (details given in Tables 1 and 2).

of the initial MLT concentration, the surface concentration of peptide remains significantly greater than that seen for the MLT-DPPC interaction at high peptide concentration. This is supported by surface pressure data where MLT adsorption from a 0.035 μM solution (data not shown) leads to an equivalent increase in surface pressure, as seen for 0.7 μM MLT adsorption to DPPC (10 mN m^{-1}).

Fig. 7 *d* gives the reflectivity profiles and associated two-layer model fits for MGN adsorption to a condensed DPPG monolayer (also provided in Table 2). At a MGN concentration of 0.7 μM, a two-layer model was required to fit the same physical model to the two isotopic contrasts. These fits revealed that the bulk of peptide resided below the lipid layer, with little or no peptide penetrating the layer. The fits do not, however, provide conclusive evidence that peptide was excluded from the lipid layer, since it was possible to fit the data to give 0%–2% of peptide in the upper lipid layer. In contrast to these findings, the MLT NR and ER-FTIR data showed that, at 0.7 μM, MLT does penetrate the lipid layer (40% within upper layer) as well as altering the lipid structure and adsorbing below the upper lipid layer. This explains the observed thicker layer found for MLT compared to MGN and CEC in Table 1.

The contrasting surface pressure and ER-FTIR results found for peptide adsorption to DPPC were also investigated using NR. Fig. 8 gives the NR profiles recorded for MLT binding to (h)- and (d)-DPPC in NRW. The condensed phase (d)-DPPC layer before peptide addition has been fitted to a single layer model, which corresponds to an area per molecule of 57 Å^2 (as seen in Table 1). This value is, within error, in agreement with surface pressure data and consistent with literature values (38,50). As shown in Fig. 8, on addition of peptide there was no significant change in the (d)-DPPC reflectivity profile, suggesting little or no MLT adsorption. However, a slight reflectivity curve was observed when MLT was adsorbed to a (h)-DPPC surface, and this suggests that the surface does in fact contain some peptide. Fitting of the reflectivity curves of the two lipid contrasts gave a single layer fit showing peptide penetration within the region of 0.1 surface fraction (10%).

DISCUSSION

Figs. 2 and 3 show apparently contrasting results between surface pressure and ER-FTIR measurements for the peptide-PC interaction. These observed differences may be due to differences in the physical properties probed by the two techniques (37). At the high lipid compressions used in this study, penetration of peptide into DPPC would conceivably lead to a large increase in surface pressure for relatively minor

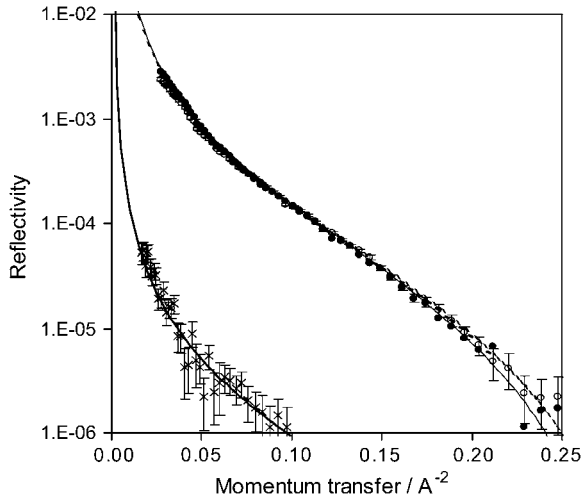

FIGURE 8 NR versus momentum transfer plot for 0.7 μM MLT adsorption to a condensed DPPC monolayer. Reflectivity profiles for peptide adsorption to chain deuterated (*solid circles*) and hydrogenated (*crosses*) DPPC are shown. Open circle symbols represent the deuterated-DPPC monolayer before peptide addition, and solid lines give best model fits to the data (details given in Table 2).

quantities of incorporated peptide (small changes in lipid compression (area per molecule)). Indeed, a surface pressure increase of 5 mN m^{-1}, as observed for MGN, would correspond to <3% lipid compression. NR fits show that the compressed lipid layer has a layer volume fraction of 0.9–0.95, allowing only limited peptide penetration. Therefore, methods sensitive to the adsorbed amount are less able to detect penetration. Consequently, ER-FTIR measurements did not show evidence of any lipid penetration unless the DPPC lipid layer compression was reduced, upon which peptide adsorption was seen, in agreement with the findings of Flach et al. (34) (data not shown). However, NR was able to confirm a weak interaction between MLT and DPPC that suggested that peptide had penetrated the lipid layer to give an interfacial layer with ~10% peptide. From our surface pressure measurements, all peptides showed some evidence of interaction with DPPC although MLT was 50% greater than the two membrane-selective peptides. Our results suggest that peptide-DPPC binding is driven by a strong interaction

TABLE 1 DPPG-peptide interaction: fit parameters for NR curves for peptide adsorption to hydrogenated DPPG in NRW (assuming $\rho_{(h)DPPG} = 0$)

Peptide concentration		Fit details: Thickness/Å	Scattering length density/10^{-6} Å^{-2}	Peptide surface excess/mg m^{-2}
MLT	0.088 μM	20	0.7	1.1
MLT	0.175 μM	28	0.7	1.5
MLT	0.7 μM	42	0.75	2.4
MGN	0.7 μM	30	1.05	2.2
CEC	0.7 μM	30	0.65	1.4

TABLE 2 Fit parameters for NR curves using (h) and (d) lipid in NRW

	Fit details: (τ) thickness/Å; (ρ) scattering length density/10^{-6} Å^{-2}	Surface excess */mg m^{-2} Lipid	Melittin
(d)-DPPC	$\tau = 21.5$, $\rho = 5.5$, A = 57 Å^2/molecule	2.3	–
DPPC + 0.7 μM MLT	$\tau_1 = 22.5$, $\rho_{(d)} = 5.5$, $\rho_{(h)} = 0.42$	2.3	0.4
(d)-DPPG	$\tau = 21$, $\rho = 5.9$, A = 55 Å^2/molecule	2.4	–
DPPG + 0.7 μM MLT	$\tau_1 = 22$, $\rho_{(d)} = 4.05$, $\rho_{(h)} = 0.71$ $\tau_2 = 24$, $\rho_{(d)} = 0.68$, $\rho_{(h)} = 0.66$ $\tau_3 = 28$, $\rho_{(d)} = 1.00$, $\rho_{(h)} = 0.05$	2.0	2.1
DPPG + 0.175 μM MLT	$\tau_1 = 22$, $\rho_{(d)} = 5.1$, $\rho_{(h)} = 0.9$ $\tau_2 = 60$, $\rho_{(d)} = 1.0$, $\rho_{(h)} = 0.05$	2.1	1.1
DPPG + 0.088 μM MLT	$\tau_1 = 24$, $\rho_{(d)} = 5.35$, $\rho_{(h)} = 0.59$	2.2	0.6
DPPG + 0.7 μM MGN	$\tau_1 = 21$, $\rho_{(d)} = 5.85$, $\rho_{(h)} = 0.36$ $\tau_2 = 22$, $\rho_{(d)} = 1.2$, $\rho_{(h)} = 1.2$	2.2	1.9

*The combined error in surface excess is ±0.1 mg m^{-2}.

with the lipid hydrocarbon chain due to the hydrophobicity of the peptide rather than interacting with the zwitterionic headgroup, and thus binding below the layer does not appear to occur.

MGN and CEC binding to DPPG appeared to be similar to that of MLT-DPPC according to the surface pressure measurements, and we believe this is because the extent of lipid compression due to peptide penetration was equivalent in the three systems. Conversely, ER-FTIR data showed large differences between the binding of the peptides to both lipid layers. As discussed above, binding to DPPC was not observed, since the technique appeared to be unable to detect low surface concentrations of inserted peptide. NR also confirmed that binding to DPPC was small, giving a surface excess of 0.4 mg m^{-2} for MLT binding to DPPC compared to 2.1 mg m^{-2} to DPPG. ER-FTIR showed that the DPPG lipid layer structure remained intact in the presence of the membrane-selective peptides; however, MLT caused the lipid layer structure to be altered. This observation was also supported by NR where both MLT and MGN have been investigated. To MGN and CEC, the peptide appears to accumulate at the headgroup of the lipid layer. Increasing the peptide concentration above 0.7 μM did not lead to increased interaction according to ER-FTIR spectroscopy. The literature supports the theory that peptide accumulates below the lipid layer but suggests that this step is before peptide penetration (12,21,24). However, in our studies we have seen

evidence of peptide penetration to DPPC without any accumulation below the lipid surface.

For each peptide, an apparent disagreement between methods is observed when considering the adsorption rates to DPPG (i.e., rate of change of surface pressure and amide I peak areas). Upon addition of peptide, surface pressure measurements show an initial sharp increase (within the first 10 min) followed by a long plateau region up to the full 3 h of adsorption. However, the amide I peak areas increase more gradually over the adsorption period, with plateau occurring after 40 and 60 min for MGN and CEC, respectively, and >3 h for MLT. This slower adsorption rate may be due to adsorption below the upper lipid layer where the increased adsorbed amount would have little effect on surface tension. The gradual changes in the amide I peak area could also be attributed to changes in the peptide orientation at the surface. MLT adsorption rate is shown to be slowest since this peptide alters the lipid layer structure and has been shown to interact with DPPG by a different mechanism.

MLT has an amphiphilic structure when in its random coil conformation, with distinct polar and hydrophobic regions, providing surfactant-like behavior that enables it to interact via different mechanisms. This amphiphilic structure is not apparent in solution for MGN and CEC, which both exhibit randomly distributed charged residues when in a random coil conformation. At an interface the peptide structures are believed to adopt a helical conformation. Our data showed adsorbed MGN to have the highest helical structure content and MLT the least. In addition, this helical conformation was observed at the air-water interface for MGN both with and without the presence of a lipid monolayer, whereas MLT did not adopt a helical conformation at the bare air-water interface. In a helical conformation, MGN and CEC possess a more pronounced amphiphatic structure than MLT with charged and hydrophobic sides to the helix (as depicted in Fig. 9) (19). This fact in the presence of a charged lipid headgroup would help drive helix formation upon adsorption. Conceivably, adsorption to the bare air-water interface would also lead to helix formation due to the amphiphilic cross section of the helix providing a hydrophobic face for adsorption and hence greater conformational stability. However, MLT's native random coil amphiphilic structure would enable it to adsorb at the air-water interface without forming a helical structure. Although Cornut et al. (32) suggested a higher helical content at the air-water interface, they also showed a tilted orientation of the peptide at the interface that would support our findings that MLT acts like a surfactant with a hydrophobic region that favors the interface.

In summary, the data presented appear to suggest that the charge distribution along the peptide is the key to the mode of interaction and interfacial behavior of the peptides. MLT's amphiphilic structure in solution (random coil conformation) enables it to adsorb without forming a helical structure. Its helix formation will therefore only occur in the case of penetration of the lipid layer possibly as a pore-forming structure at membrane surfaces. A central proline residue gives MLT a kink in its helical structure that would potentially play a role in its lipid insertion properties (19). MGN has what appears to be a random polar and charged amino acid sequence in solution (random coil), and therefore the presence of an interface promotes helical formation and the formation of an amphiphatic structure that can orientate at an interface to maximize interaction. Although the amphiphatic nature of the CEC helix is less pronounced than that of MGN, it does have the structural characteristics to explain the fact that it behaves similarly to MGN but with reduced interaction and surface activity.

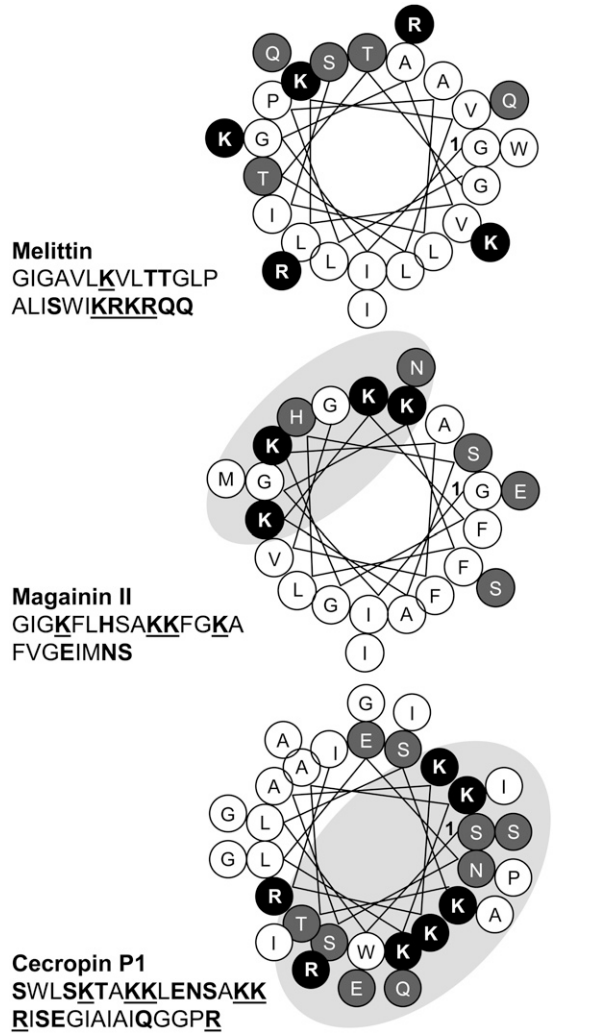

FIGURE 9 Helical wheel projections for MLT, MGN, and CEC. The beginning of the helix is marked with 1 and the residues are coded as hydrophobic (*white*), polar (*shaded*), and cationic (*black*). The peptide sequences are also shown with polar residues bold and cationic residues underlined.

This work was funded by the Leverhulme Trust and the Engineering and Physical Sciences Research Council.

REFERENCES

1. Gabay, J. E. 1995. Ubiquitous natural antibiotics. *Science*. 264:373–374.

2. Hancock, R. E. W. 1999. Host defense (cationic) peptides: what is their future clinical potential? *Drugs.* 57:469–473.
3. Yeaman, M. R., and N. Y. Yount. 2003. Mechanisms of antimicrobial peptide action and resistance. *Pharmacol. Rev.* 55:27–55.
4. Boman, H. G. 2003. Antibacterial peptides: basic facts and emerging concepts. *J. Intern. Med.* 254:197–215.
5. Zasloff, M. 1987. Magainins, a class of antimicrobial peptides from Xenopus skin: isolation, characterization of two active forms, and partial cDNA sequence of a precursor. *Proc. Natl. Acad. Sci. USA.* 84:5449–5453.
6. Dempsey, C. E. 1990. The actions of melittin on membranes. *Biochim. Biophys. Acta.* 1031:143–161.
7. Shai, Y. 1999. Mechanism of the binding, insertion and destabilization of phospholipid bilayer membranes by alpha-helical antimicrobial and cell non-selective membrane-lytic peptides. *Biochim. Biophys. Acta.* 1462:55–70.
8. Bechinger, B. 2004. Structure and function of membrane-lytic peptides. *CRC Crit. Rev. Plant Sci.* 23:271–292.
9. Epand, R. M., and H. J. Vogel. 1999. Diversity of antimicrobial peptides and their mechanisms of action. *Biochim. Biophys. Acta.* 1462:11–28.
10. Papo, N., and Y. Shai. 2003. Exploring peptide membrane interaction using surface plasmon resonance: differentiation between pore formation versus membrane disruption by lytic peptides. *Biochem.* 42:458–466.
11. Dawson, C. R., A. F. Drake, J. Helliwell, and R. C. Hider. 1978. The interaction of bee melittin with lipid bilayer membranes. *Biochim. Biophys. Acta.* 510:75–86.
12. Ludtke, S. J., K. He, Y. Wu, and H. W. Huang. 1994. Cooperative membrane insertion of magainin correlated with its cytolytic activity. *Biochim. Biophys. Acta.* 1190:181–184.
13. Brauner, J. W., R. Mendelsohn, and F. G. Prendergast. 1987. Attenuated total internal reflectance Fourier-transform infrared studies of the interaction of melittin, 2-fragments of melittin, and delta-hemolysin with phosphocholines. *Biochem.* 26:8151–8158.
14. Blondelle, S. E., B. Forood, R. A. Houghten, and E. Perez-Paya. 1997. Secondary structure induction in aqueous vs membrane like environments. *Biopolymers.* 42:489–498.
15. Asthana, N., S. P. Yadav, and J. K. Ghosh. 2004. Dissection of antibacterial and toxic activity of melittin. *J. Biol. Chem.* 279:55042–55050.
16. Lee, T. H., H. Mozsolits, and M. I. Aguilar. 2001. Measurement of the affinity of melittin for zwitterionic and anionic membranes using immobilized lipid biosensors. *J. Pept. Res.* 58:464–476.
17. Frey, S., and L. K. Tamm. 1991. Orientation of melittin in phospholipid bilayers. A polarized attenuated total reflection infrared study. *Biophys. J.* 60:922–930.
18. Habermann, E., and J. Jentsch. 1967. Bee and wasp venom: the biochemistry and pharmacology of their peptides and enzymes are reviewed. *Science.* 177:314–322.
19. Dathe, M., and T. Wieprecht. 1999. Structural features of helical antimicrobial peptides: their potential to modulate activity on model membranes and biological cells. *Biochim. Biophys. Acta.* 1462:71–87.
20. Matsuzaki, K., K. Sugishita, N. Fujji, and K. Miyajima. 1995. Molecular basis for membrane selectivity of an antimicrobial peptide, magainin 2. *Biochem.* 34:3423–3429.
21. Bechinger, B., M. Zasloff, and S. J. Opella. 1993. Structure and orientation of the antibiotic peptide magainin in membranes by solid-state nuclear-magnetic-resonance spectroscopy. *Protein Sci.* 2:2077–2084.
22. Ludtke, S. J., K. He, W. T. Heller, T. A. Harroun, L. Yang, and H. W. Huang. 1996. Membrane pores induced by magainin. *Biochem.* 35:13723–13728.
23. Matsuzaki, K., Y. Mitani, K. Akada, O. Murase, S. Yoneyama, M. Zasloff, and K. Miyajima. 1998. Mechanism of synergism between antimicrobial peptides magainin 2 and PGLa. *Biochemistry.* 37:15144–15153.
24. Tachi, T., R. F. Epand, and K. Matsuzaki. 2002. Position dependent hydrophobicity of the antimicrobial magainin peptide affects the mode of lipid-peptide interactions and selectivity toxicity. *Biochemistry.* 41:10723–10731.
25. Steiner, H., D. Andreu, and R. B. Merrifield. 1988. Binding and action of cecropin and cecropin analogues: antibacterial peptides from insects. *Biochim. Biophys. Acta.* 939:260–266.
26. Marassi, F. M., S. J. Opella, P. Juvvadi, and R. B. Merrifield. 1999. Orientation of cecropin A helices in phospholipid bilayers determined by solid-state NMR spectroscopy. *Biophys. J.* 77:3152–3155.
27. Gazit, E., A. Boman, H. G. Boman, and Y. Shai. 1995. Interaction of the mammalian antibacterial peptide cecropin P1 with phospholipid vesicles. *Biochem.* 34:11479–11488.
28. Gazit, E., I. R. Miller, P. C. Biggin, M. S. P. Sansom, and Y. Shai. 1996. Structure and orientation of the mammalian antibacterial peptide cecropin P1 within phospholipid membranes. *J. Mol. Biol.* 258:860–870.
29. Christensen, B., J. Fink, R. B. Merrifield, and D. Mauzerall. 1988. Channel forming properties of cecropins and related model compounds incorporated into planar lipid membranes. *Proc. Natl. Acad. Sci. USA.* 85:5072–5076.
30. Saccini, J., S. Castano, F. Beaurain, M. Laguerre, and B. Desbat. 2004. Stabilization of phospholipid multilayers at the air-water interface by compression beyond the collapse: a BAM, PM-IRRAS, and molecular dynamics study. *Langmuir.* 20:9190–9197.
31. Hristova, K., C. E. Dempsey, and S. H. White. 2001. Structure, location, and lipid perturbations of melittin at the membrane interface. *Biophys. J.* 80:801–811.
32. Cornut, I., B. Desbat, J. M. Turlet, and J. Dufourcq. 1996. In situ study by polarization modulated Fourier transform infrared spectroscopy of structure and orientation of lipids and amphipathic peptides at the air-water interface. *Biophys. J.* 70:305–312.
33. Mendelsohn, R., J. W. Brauner, and A. Gericke. 1995. External infrared reflection-absorption spectrometry monolayer films at the air-water interface. *Annu. Rev. Phys. Chem.* 46:305–334.
34. Flach, C. R., F. G. Prendergast, and R. Mendelsohn. 1996. Infrared reflection-absorption of melittin interaction with phospholipid monolayers at the air/water interface. *Biophys. J.* 70:539–546.
35. Flach, C. R., J. W. Brauner, J. W. Taylor, R. C. Baldwin, and R. Mendelsohn. 1994. External reflection FTIR of peptide monolayer films in-situ at the air/water interface. *Biophys. J.* 67:402–410.
36. Lad, M. D., F. Birembaut, R. A. Frazier, and R. J. Green. 2005. Protein-lipid interactions at the air/water interface. *Phys. Chem. Chem. Phys.* 7:3478–3485.
37. Lad, M. D., F. Birembaut, J. M. Matthew, R. A. Frazier, and R. J. Green. 2006. Protein structural change during adsorption to the air/water interface. *Phys. Chem. Chem. Phys.* 8:2179–2186.
38. Vaknin, D., K. Kjear, J. Alsnielsen, and M. Losche. 1991. Structural-properties of phosphatidylcholine in a monolayer at the air-water interface: neutron reflection study and reexamination of x-ray reflection measurements. *Biophys. J.* 59:1325–1332.
39. Maierhofer, A. P., D. G. Bucknall, and T. M. Bayerl. 2000. Modulation of cytochrome C coupling to anionic lipid monolayers by a change of the phase state: a combined neutron and infrared reflection study. *Biophys. J.* 79:1428–1437.
40. Lee, J. Y., A. Boman, S. Chanxin, M. Andersson, H. Jornvall, V. Mutt, and H. G. Boman. 1989. Antibacterial peptides from pig intestine: isolation of a mammalian cecropin. *Proc. Natl. Acad. Sci. USA.* 86:9159–9162.
41. Penfold, J., R. M. Richardson, A. Zarbakhsh, J. Webster, D. G. Bucknall, A. R. Rennie, R. A. L. Jones, T. Cosgrove, R. K. Thomas, J. S. Higgins, R. D. I. Fletcher, E. J. Dickinson, S. J. Roser, I. A. McLure, A. R. Hillman, R. W. Richards, E. J. Staples, A. N. Burgess, E. A. Simister, and J. W. Whites. 1997. Recent advances in the study of chemical surfaces and interfaces by specular neutron reflection. *J. Chem. Soc. Faraday Trans.* 93:3899–3917.
42. Green, R. J., T. J. Su, H. Joy, and J. R. Lu. 2000. Interaction of lysozyme and sodium dodecyl sulfate at the air-liquid interface. *Langmuir.* 16:5797–5805.

43. Green, R. J., T. J. Su, J. R. Lu, and J. R. P. Webster. 2001. The displacement of pre-adsorbed protein with a cationic surfactant at the hydrophilic SiO2-water interface. *J. Phys. Chem. B*. 105:9331–9338.

44. Green, R. J., T. J. Su, J. R. Lu, and J. Penfold. 2001. The interaction between SDS and lysozyme at the hydrophilic solid-water interface. *J. Phys. Chem. B*. 105:1594–1602.

45. Born, M., and E. Wolf. 1970. Principles of Optics. Pergamon Press, Oxford, UK.

46. Tripp, B. C., J. J. Magda, and J. D. Andrade. 1995. Adsorption of globular-proteins at the air/water interface as measured via dynamic surface-tension: concentration-dependence, mass-transfer considerations, and adsorption-kinetics. *J. Colloid Interface Sci*. 173:16–27.

47. Diederich, A., C. Sponer, D. Pum, U. B. Sleytr, and M. Losche. 1996. Reciprocal influence between the protein and lipid components of a lipid-protein membrane model. *Colloids Surf. B Biointerfaces*. 6:335–346.

48. Sui, S. F., H. Wu, Y. Guo, and K. S. Chen. 1994. Conformational-changes of melittin upon insertion into phospholipid monolayers and vesicles. *J. Biochem. (Tokyo)*. 116:482–487.

49. Dubreil, L., V. Vie, S. Beaufils, D. Marion, and A. Renault. 2003. Aggregation of puroindoline in phospholipid monolayers spread at the air-liquid interface. *Biophys. J*. 85:2650–2660.

50. Polverini, E., S. Arisi, P. Cavatorta, T. Berzina, L. Cristofolini, A. Fasano, P. Riccio, and M. P. Fontana. 2003. Interaction of myelin basic protein with phospholipid monolayers: mechanism of protein penetration. *Langmuir*. 19:872–877.